IEEE Access
Multidisciplinary | Rapid Review | Open Access Journal

Received December 5, 2017, accepted January 10, 2018, date of publication February 6, 2018, date of current version March 15, 2018.

Digital Object Identifier 10.1109/ACCESS.2018.2799304

A Sub-Nyquist Radar Electronic Surveillance System

JEONG PARK[1], JEHYUK JANG[1], SANGHUN IM[2], AND HEUNG-NO LEE[1], (Senior Member, IEEE)

[1]School of Electrical Engineering and Computer Science, Gwangju Institute of Science and Technology, Gwangju 61005, South Korea
[2]Hanwha Systems, Seongnam 13524, South Korea

Corresponding author: Heung-No Lee (heungno@gist.ac.kr)

This work was supported by a grant-in-aid of Hanwha Systems.

ABSTRACT The modulated wideband converter (MWC) is well-known for a sub-Nyquist wideband sampling capability based on compressed sensing (CS) theory. In this paper, our goal is to use the MWC as a base to design a sub-Nyquist radar electronic surveillance (ES) system. Our focus is then to extend the capabilities of the previous MWC system in order to meet the challenges, i.e., a very long acquisition time, a much larger simultaneous monitoring bandwidth, and a faster digital signal processing receiver. To this end, we present a new performance analysis framework and then a new digital domain receiver. The proposed performance analysis framework will be useful in comparing signal-acquisition performance of the proposed ES system with those of other sub-Nyquist receivers, including those of the classical Nyquist rate receivers, without resorting to extensive simulations. This framework can also be used to study the complex interplays of important system parameters of MWC, such as the sampling rate, the number of parallel channels, the period of Pseudo random sequence, and thus guides us in selecting the right system dimensions and parameters for desired performance. Radar surveillance application has its inherent needs for very long acquisition time and simultaneous monitoring of very large frequency range. To meet this challenge, a fast signal recovery system needs to be developed, so that radar signal logistics can be retained and recovered from compressed samples. We have proposed a split and synthesis process in which the radar signal recovery problem over a long signal acquisition time can be divided into many small CS signal recovery problems, and the solutions for small pieces are put together later on at the end. In addition, a sub-sampling method is proposed to have the multiple measurement vector problem complete signal recovery faster without noticeable performance loss.

INDEX TERMS Compressed sensing, electronic surveillance, modulated wideband converter, multiple measurement vectors, radar signal.

I. INTRODUCTION

Electronic surveillance (ES) systems monitor radar signals emitted from opponent radar systems, which detect subjects by transmitting radar signals and receiving them when reflected back from the subjects. Radar ES systems are useful for recognizing the intent of a threat in advance. Opponent radar signals are spectrally sparse, spread around a wide frequency band, and are unknown in advance, presenting unique challenges for signal processing.

Radar ES systems can utilize a Nyquist-rate receiver, such as the rapidly swept superheterodyne receiver (RSSR) [1], [2]. RSSR chronologically samples the sub-bands of a wideband region. However, RSSR inevitably misses some of the signals. For wideband signals, the sweeping period must be relatively long, though opponent radar signals are brief in duration. As shown in Fig. 1, although a signal may appear in some frequency bands for a while, the RSSR's sweep samples empty sub-bands and fails to catch the signal. The inevitable failure of catching some signals from the RSSR sweep can become a critical problem depending on its applications such as detecting missiles and monitoring hostile aircraft.

To take samples of spectrally sparse signals at a rate far below the Nyquist rate without information losses, the modulated wideband converter (MWC) [3], [4] and random modulation pre-integration (RMPI) [5], [6] have been proposed.

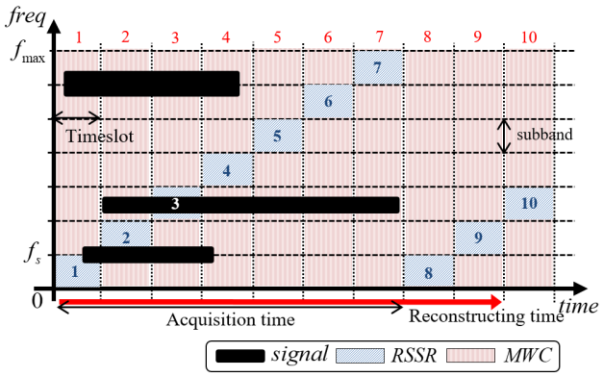

FIGURE 1. Signal model and signal acquisition schemes of the RSSR and MWC denoted as blue and red colored integers, respectively.

Based on the compressive sensing (CS) theory [7], [8], both systems compress the received spectrum by mixing it with rapidly alternating pseudo-random sequences, takes the low-rate samples over a certain acquisition time, and finally reconstructs the original spectrum from the collected samples in the digital domain. We aim to design an ES system based on MWC.

Notably, in terms of the probability of successful signal acquisition, MWC has not been compared with other sub-Nyquist receivers or conventional Nyquist receivers with similar hardware costs. To this end, one can construct prototypes and repeat hundreds of signal-acquisition tests. However, that is inefficient and expensive. Thus, a performance analysis model which predicts the signal acquisition performance of systems with similar hardware costs will be of highly valuable.

In the ES scenario, owing to tactical purposes such as the avoidance of reverse tracing by the enemy, modern radar systems frequently switch their signal characteristics. The longer radar samples are acquired, the more information of foe's intention can be scrutinized. In the ES system exploiting MWC, since CS reconstruction algorithms deal with only a finite length of compressed sample, the reconstructed samples possibly contain only a portion of a radar signal. Hence, for MWC to retain sufficient amount of information for the intention analysis, a sufficiently long acquisition time is needed. A CS signal reconstruction algorithm covering the entire acquisition time would give the best performance, but such an algorithm would require a very high computational complexity. To compound the matter, the signal bandwidth we aim to study is very large as well. As radar systems cover very wide frequency regions including C-band (4-8GHz), X-band (8-12GHz) and Ku-band (12-18GHz) [9], the bandwidth of interest for simultaneous monitoring purpose needs to be wider than the 2GHz bandwidth of the previously studied MWC [3]. As the result, the radar ES system we aim to study in this paper requires very large system dimension for any CS signal reconstruction algorithm to work. Large system dimension entails high computational complexity. Our goal therefore is to focus on how to divide the observation time into small segments of time to reduce complexity of signal reconstruction, and how to put the segmented signals of interest together without losing quality.

Our contributions in this paper are two fold, one is a novel signal-acquisition probability analysis and a low complexity radar ES system design for very wide bandwidth monitoring applications. First, we present a new performance evaluation framework which allows analytic comparison of the signal-acquisition performances of several wideband signal receivers. This allows us to compare receiver architectures while avoiding realization of all the receivers and exhaustive testing in simulation. Our analysis demonstrates the specific benefits of MWC over conventional RSSR. In addition, the analytic method can be applied to other sub-Nyquist receivers based on CS. For example, analysis applied on RMPI is included. This framework can also return design parameters for the radar ES system.

Second, the design of a low complexity and a wideband monitoring ES receiver using MWC is presented in this paper. We show how a long acquisition time is divided into continuously disjoint timeslots, how a CS reconstruction algorithm works for each segment in a single time slot, and how all of the reconstructed segments are synthesized. We call this split and synthesis process and show this effort reduces the total computational complexity required for reconstruction of radar signals for a long acquisition time at the cost of slight degradation in reconstruction performance. In addition, a sub-sampling method is presented aiming to further reduce the computational complexity of a CS reconstruction algorithm working within a time slot. Namely, the subsamples are selected based on the principle components of the received signal.

In Section II, we briefly introduce wideband signal receivers, including RSSR, RMPI, and MWC, and formulate problems for the radar ES system. Section III details the analysis of signal-acquisition probabilities. Section IV presents our sub-Nyquist radar ES system design, including the split-process and synthesis process. A pre-processing method for the CS reconstruction algorithm is detailed in Section V. Sections VI and VII present the results of our simulations and our conclusions, respectively.

II. PROBLEM FORMULATION AND BACKGROUND

The input $x(t)$ is modeled as an aggregation of radar signals generated from a range of radar systems. In particular, the input is defined by the following equation:

$$x(t) = \sum_{i=1}^{N} r_i(t), \quad 0 \le t < \infty, \tag{1}$$

where $r_i(t)$ is a radar signal from the i-th radar system and is located widely within $\mathcal{F}_{NYQ} = [-f_{\max}, f_{\max}]$, where $f_{\max}$ can be of the order of GHz. Including the carrier frequencies, the pulse description words (PDWs) such as pulse repetition intervals (PRIs), time-of-arrivals (TOAs), time-of-departures (TODs), pulse widths, and duty cycles are unknown *a priori*. For each $r_i(t)$, we model the carrier frequency ranges within $[0, f_{\max})$, and the bandwidth B_i is

truncated to $B_{\min} \leq B_i \leq B_{\max}$. For separable $r_i(t)$, we assume that the spectra of $r_i(t)$ are disjointed. In addition, the aggregation $x(t)$ is sparse in the frequency domain, i.e., $2NB_{\max} \ll f_{\max}$. Briefly, we acquire a successively incoming signal $x(t)$, which is regarded as a spectrally sparse multiband signal [3] with unknown parameters.

A. RAPIDLY SWEPT SUPERHETERODYNE RECEIVER

The RSSR [1] is a representative Nyquist receiver designed to cover wideband regions with a low rate of analog-to-digital convertors (ADC). RSSR receives a multiband signal and divides the entire spectrum into multiple subbands by exploiting a bank of bandpass filters. The subbands are then sampled by an ADC. With time-division multiplexing [2], RSSR chronologically takes time-domain samples of the subbands in sequence. The blue boxes in Fig. 1 depict the time-division multiplexing, where the numbered regions in time-frequency domain are the signal acquiring subbands of RSSR.

Despite the simple system structure of RSSR, in Fig. 1, it inevitably fails to acquire some of radar signals outside the current acquiring subband. One can reduce the failures of signal acquisitions by using faster ADC in the state of the art [10], but such ADC have many implementation problems such as prohibitive cost, high energy consumption, low memory, and low ADC resolution [6], [11]. The implementation limits also restricts to wider the bandwidth $f_{\max}$ of signal acquisition. Intuitively, the probability that RSSR fails to acquire the whole radar signals would increase as the number of signals and/or the range of the input spectrum increases. In Section III, we compute the probability of successful signal acquisition by RSSR.

B. RANDOM MODULATION PRE-INTEGRATION

RMPI [5] is a channelized sub-Nyquist receiver that acquires a multiband signal at one acquisition time T_{acq}. For each channel, the multiband signal is mixed with a pseudorandom (PR) sequence and the result is then integrated. An ADC samples the mixed result at the sub-Nyquist rate f_s after the integrating module. If m is the number of channels, the channel-end sampling rate [6] f_{bs} is defined as follows:

$$f_{bs} \triangleq mf_s. \tag{2}$$

With the system matrix from the analog architecture, RMPI reconstructs multiband signal with a CS algorithm. However, because the matrix is block diagonal in form, the system matrix is considerably large to compute expeditiously. For one block, the number of rows and columns corresponds to the number of channels and f_{nyq}/f_s respectively, and each block is repeated f_{nyq}/f_{bs} times. This large block-diagonal matrix causes high computational complexity and long reconstruction times, which renders RMPI impractical for the ES applications.

In addition, the range of the sample sequence containing signal information corresponds to Nyquist frequency and is digitized at an interval of $1/T_{acq}$. Hence, for N given signals and a minimum bandwidth $B_{\min}$, the number of nonzero entries in a sampled sequence is more than $2NB_{\min}T_{acq}$. The large number of nonzero entries impedes RMPI's signal-acquisition performance.

C. MODULATED WIDEBAND CONVERTER

To resolve missing signals in the RSSR and avoid the computational limits of RMPI, we examined the MWC [3] for ES, which comprises analog and digital modules. In the analog module, the MWC takes samples containing compressed information of $x(t)$ at a rate below the Nyquist rate. In the digital module, the post-digital signal process (DSP) and a CS recovery algorithm reconstruct the compressed samples into the Nyquist-rate sample of $x(t)$.

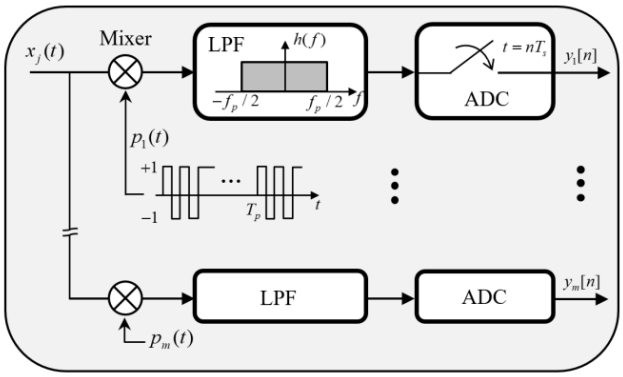

FIGURE 2. Analog module of the MWC.

The analog module of the MWC comprises m channels, including a series of mixers, low-pass filters (LPFs), and ADCs, as shown in Fig. 2. For each channel, the multiband signal is mixed with a T_p-periodic PR sequence, $p_i(t)$. The spectrum of the sequence has $M = 2M_0 + 1$ weighted impulses at intervals of $f_p = T_p^{-1}$. The mixed signal passes through an anti-aliasing LPF whose cutoff frequency is defined as $f_s/2 = qf_p/2$, where $q = 2q_0 + 1 > 0$ is an odd integer. As a result, the mixer and LPF divide the input frequency range $[-f_{\max} - q_0 f_p, f_{\max} + q_0 f_p]$ into $L = 2L_0 + 1$ sub-bands at intervals of f_p, as presented in [3]. The sub-bands are then compressed by multiplying them with the Fourier coefficients $c_{i,l}$ of the PR sequence and projecting into $[-f_s/2, f_s/2)$. Next, the ADC samples the compressed sub-bands at the rate of f_s. For the i-th channel, the discrete-time Fourier transform (DTFT) of the output of the ADC can be expressed by

$$\breve{y}_i\left(e^{j2\pi f T_s}\right) = \sum_{l=-L_0}^{L_0} c_{i,l}\mathbf{X}(f - lf_p) \tag{3}$$

for $-f_s/2 \leq f < f_s/2$ [3]. From the projection into $[-f_s/2, f_s/2)$, the information from $q = f_s/f_p$ subbands are piled in a single row of the $\mathbf{X}$ matrix. Note that $M \leq L$ Fourier coefficients of $p_i(t)$ are unique and $q - 1 = L - M$ coefficients are repetitions. The MWC then reconstructs the Nyquist sample of $x(t)$ from the compressed samples in the digital module of the MWC.

In the DSP, the channel expansion method [3] is applied to extend the number of the equation (3) by disjointing the correlations of the $q-1$ repeated Fourier coefficients $c_{i,l}$. The channel expansion method is represented by the following equation:

$$\begin{aligned}\breve{y}_{i,k}[\widehat{n}] &= (y_i[n]e^{-j2\pi k f_p n T_s}) * h_D[n]\Big|_{n=\tilde{n}q} \\ &= (y_i[n]e^{-j2\pi kn/q}) * h_D[n]\Big|_{n=\tilde{n}q}, \end{aligned} \tag{4}$$

where $k \in \{-q_0, \cdots, q_0\}$. As shown in (4), for each k, $y_i[n]$ is modulated with a different frequency kf_p and convoluted with q LPFs $h_D[n]$, whose cutoff frequencies are π/q. The sequence is then decimated by q. As a result, the outcome of channel expansion is

$$\breve{\mathbf{Y}}_i\left(e^{j2\pi f T_p}\right) = \sum\nolimits_{l=-M_0}^{M_0} c_{i,(l+k)}\mathbf{X}(f - lf_p) \tag{5}$$

for $-f_p/2 \leq f \leq f_p/2$. Consequently, we can obtain mq equations from m analog channels. With the continuous-to-finite (CTF) block in [3], the DTFT $\breve{\mathbf{Y}}_i\left(e^{j2\pi f T_p}\right)$ becomes a finite sequence. For m channels, (5) can be expressed as follows:

$$\breve{\mathbf{Y}}[n] = \breve{\mathbf{C}}\breve{\mathbf{Z}}[n], \tag{6}$$

where the measurement matrix $\breve{\mathbf{Y}} \in \mathbb{R}^{mq\times v}$ corresponds to the output from the MWC, $\breve{\mathbf{C}} \in \mathbb{C}^{mq\times M}$ is the sensing matrix, $\breve{\mathbf{Z}} \in \mathbb{R}^{M\times v}$ contains the signal information, v is the length of column in $\breve{Y}$ yielded from the CTF block, and $M = 2M_0 + 1$. The matrix equation (6) is exploited to reconstruct the multiband signal through a CS recovery algorithm, at which point the MWC has successfully acquired signals.

The main difference between the MWC and RMPI is how to sparsify the original continuous spectrum. First, the CS model of RMPI discretizes the continuous spectrum at the Nyquist rate. Since the received spectrum in the ES scenario usually consists of disjoint continuous narrow bands, the discretization of such a spectrum yields not only a huge size of CS model but also high sparsity. CS theory states the sparse reconstruction of the original spectrum is successful only for a low sparsity. While, the CS model of MWC divides the continuous spectrum into disjoint subbands $X\left(f - lf_p\right)$ for $l \in \{-M_0, \cdots, M_0\}$ at intervals f_p. The sparsity of MWC is counted as the number of nonzero subbands, where the spectra of radar signals $r_i(t)$ are contained. With the low sparsity and the small size of CS model, we design an ES system based on MWC.

D. PROBLEM FORMULATION

Although MWC was designed to acquire a multiband signal, this architecture is difficult to directly implement in a radar ES system. Radar ES faces a tradeoff between acquisition time and post-processing time. When the acquisition time is shorter than the post-processing time, the ES system faces a bottleneck in outputting the acquired signal. As a result, continuous incoming signals stack up and are not included in the output. Meanwhile, the reconstruction process includes complex computations in both the DSP and CS algorithms. In the DSP, for a given compressed sample length v, the computational complexity of (4) is a function of $O\left(v^2\right)$, which grows as $v \triangleq T_{acq}/T_s$ increases. One option to reduce computational complexity would be to increase the sampling period T_s of the ADC and/or reduce the acquisition time T_{acq} to reduce the length v. However, increasing the sampling period is impractical because it reduces the channel expansion factor q in (4). With the reduced q, the channel expansion method is no longer useful. Moreover, the acquisition time cannot be reduced. Because opponent radar systems frequently change their radar signal characteristics, a radar ES system is needed to acquire signals over a long acquisition time to efficiently detect an enemy radar system. Another option would involve dividing a long acquisition time into several timeslots to reduce computational complexity. However, this division scheme raises the problem of time-aliasing [12]. When segments of a long signal are processed individually and concatenated into the original signal, time-aliasing degrades the reconstructed signal at the borders of the segments. If we resolve the time-aliasing problem, we can greatly reduce computational complexity with sufficiently accurate reconstruction.

Processing a large number of samples acquired over a long acquisition time entails high computational complexity in the CS recovery algorithm. The problem of (6) in the MWC is referred to as the multiple measurement vector (MMV) problem, and the computational complexity of the algorithm is greatly influenced by the size of the measurement matrix. By reducing the measurement matrix without missing signals, computational complexity can be reduced for the radar ES system.

III. SIGNAL-ACQUISITION PROBABILITY ANALYSIS

This section compares the signal acquisition performances of the MWC, RMPI, and RSSR using a novel probability analysis. These receivers aim to watch out a very wide bandwidth of frequencies where unknown radar signals of interest may exist. Signals of no interest can be removed from consideration easily for the receivers, such as radar signals from friendly forces and commercial signals. In this analysis, therefore, for the frequency bands of interest, we assume uniform distribution of the occurrences of unknown carrier frequencies. We also assume that receivers aim to receive multiple radar signals each having bandwidth of B Hz over a very wide range of frequencies up to f_{nyq}. From the analytic results, we observe that the analysis guides the design of system parameters such as the number of channels m, the ADC sampling rate f_s, and the cycle of PR sequence f_p^{-1}. Our analytic method allows for instant comparisons without building and simulating each receiver.

From the perspective of sampling theory, the success of lossless sub-Nyquist sampling by the MWC at a given sampling rate depends proportionally on the sum of the bandwidths of the occupied sub-bands. Hence, once we learn the number of occupied sub-bands, we can expect successful

lossless acquisition for a given number of input signals. To calculate the probability of successful signal acquisition, we generate random variables representing the numbers of input signals, split spectra, and totally occupied sub-bands and derive their distributions.

First, we derive a lower bound of probability for signal acquisition via the MWC. Let X denote the number of received signals in a timeslot and Y denote split signals. Then, the conditional probability mass function (PMF) of Y given X can be defined as follows:

$$P_{Y|X}(y|x) = {}_xC_y \left(p_{s,MWC}\right)^y \left(1 - p_{s,MWC}\right)^{x-y}, \tag{7}$$

where p_s is the probability that a signal is split by the grid of sub-bands. By assuming that the carrier frequency of the signal can be uniformly drawn, we calculate p_s using the equation of:

$$\begin{aligned} p_{s,MWC} &= 1 - \sum_{i=-M_0}^{M_0} \int_{if_p - \frac{f_p}{2} + \frac{B}{2}}^{if_p + \frac{f_p}{2} - \frac{B}{2}} \frac{1}{f_{NYQ}} dx \\ &= \frac{B}{f_p}, \end{aligned} \tag{8}$$

where $B < f_p$ is the bandwidth of each signal. Focusing on the positive sub-bands corresponding to real signals, the number of split and un-split spectra occupants K can be defined as $K = (X - Y) + 2Y = X + Y$. Note that the occupants do not overlap. The conditional PMF of occupant K is expressed as

$$\begin{aligned} P_{K|X}(k|x) &= P_{X+Y|X}(x + y|x) \\ &\equiv P_{Y|X}(y|x) \\ &= P_{Y|X}(k - x|x). \end{aligned} \tag{9}$$

The moment generating function of the occupant is derived as follows:

$$\begin{aligned} &M_{K|X}(\mu_x) \\ &= \sum_{k=x}^{2x} e^{\mu_x k} \cdot P_{K|X}(k|x) \\ &= \sum_{k=x}^{2x} e^{\mu_x k} \cdot P_{Y|X}(k - x|x) \\ &= \sum_{k=x}^{2x} e^{\mu_x k} \cdot {}_xC_{k-x} \left(p_{s,MWC}\right)^{k-x} \left(1 - p_{s,MWC}\right)^{x-(k-x)} \end{aligned} \tag{10}$$

Assuming that the MWC achieves lossless sub-Nyquist sampling if and only if $K \leq \kappa_{MWC}$, using the Chernoff bound, the lower bound of successful sampling is obtained by the following equation:

$$\begin{aligned} &P_{MWC}(\text{Successful sampling}) \\ &\quad = P_{K|X}(k \leq \kappa_{MWC}|x) \\ &\quad > 1 - \min_{\mu_x \geq 0} e^{-\mu_x \kappa_{MWC}} M_{K|X}(\mu_x), \end{aligned} \tag{11}$$

where κ_{MWC} is the maximum sparsity that allows the CS problem to be exactly solved. κ_{MWC} can be determined by the equation in [3], which can be written as follows:

$$mq \approx 2\kappa_{MWC} \log\left(M/\kappa_{MWC}\right). \tag{12}$$

As presented in [13], the parameters μ_x can be obtained by solving the following equation:

$$\mu_x = \arg\min_{\mu_x \geq 0} \left(\ln\left(E[e^{\mu_x x}]\right) - \mu_x \kappa_{MWC}\right). \tag{13}$$

By substituting κ_{MWC} and the last expressions of (8) and (10) into (11), the lower bound of successful sampling can be expressed in terms of system parameters:

$$\begin{aligned} &P_{MWC}(\text{Successful sampling}) \\ &> 1 - \min_{\mu_x \geq 0} e^{-\mu_x \kappa_{MWC}} \left(\frac{f_p - B}{\sqrt{B f_p}}\right)^{2x} \sum_{k=x}^{2x} {}_xC_{k-x} \left(\frac{e^{\mu_x} B}{f_p - B}\right)^k \end{aligned} \tag{14}$$

Note that $f_p = f_{nyq}/M$.

Second, we derive the probability of signal acquisition for the RMPI. Owing to the architecture of the RMPI, the occupants correspond to digitized signal bands B/T_{acq}^{-1} among the digitized Nyquist range f_{nyq}/T_{acq}^{-1}. For N received signals, the signals occupy at least $N\lfloor BT_{acq}\rfloor$ slots. Because the band is not always exactly fit to the digitized graduation, the probability of extra occupants exceeds a portion of B compared to the width of the minimum occupants $T_o^{-1}\lfloor BT_{acq}\rfloor$ at one bin T_{acq}^{-1}, i.e.,

$$p_{s,RMPI} = \left(B - T_{acq}^{-1}\lfloor BT_{acq}\rfloor\right)/T_{acq}^{-1} = BT_{acq} - \lfloor BT_{acq}\rfloor. \tag{15}$$

We then express the maximum recoverable sparsity of RMPI κ_{RMPI} as $m_{RMPI}/2 = f_{nyq}/2f_s$. For the l_0 minimization problem, which is the optimal but mathematically intractable solver, the algorithm estimates the sparsity as half of the number of equations [14]. If the RMPI fails to acquire a signal with higher κ_{RMPI} than κ_{MWC}, MWC is superior. As found in (11), the RMPI fails at sampling when the minimum occupants $N\lfloor BT_{acq}\rfloor > \kappa_{RMPI}$ and succeeds when the maximum occupants $N\left(\lfloor BT_{acq}\rfloor + 1\right) < \kappa_{RMPI}$. In the remaining cases, the probability of successful sampling is the complement of the sampling failure, which is the number of occupants over κ_{RMPI} with $p_{s,RMPI}$. Consequently, the probability of successful sampling for RMPI can be expressed as follows:

$$\begin{aligned} &P_{RMPI}(\text{Successful sampling}) \\ &= \begin{cases} 0, & \lfloor BT_{acq}\rfloor > \kappa_{RMPI} \\ 1, & N(\lfloor BT_{acq}\rfloor + 1) < \kappa_{RMPI} \\ 1 - \sum_{i=\lceil \kappa_{RMPI} - N\lfloor BT_{acq}\rfloor \rceil}^{N} p_{s,RMPI}^i, & o.w. \end{cases} \end{aligned} \tag{16}$$

Lastly, we calculate the signal-acquisition probability for the RSSR. Because only the information of signals whose spectrum is fully located in a band currently being acquired

by an activated filter bank is preserved in the output samples from the RSSR, the probability of successful acquisition under the assumption of uniform distribution of the signals in the frequency domain can be described by the following equation:

$$P_{RSSR}\,(\text{Successful Sampling}) = \left(\frac{W_{BPF} - B}{f_{nyq}/2 - B}\right)^{x}, \qquad (17)$$

where W_{BPF} is the bandwidth of the filter banks.

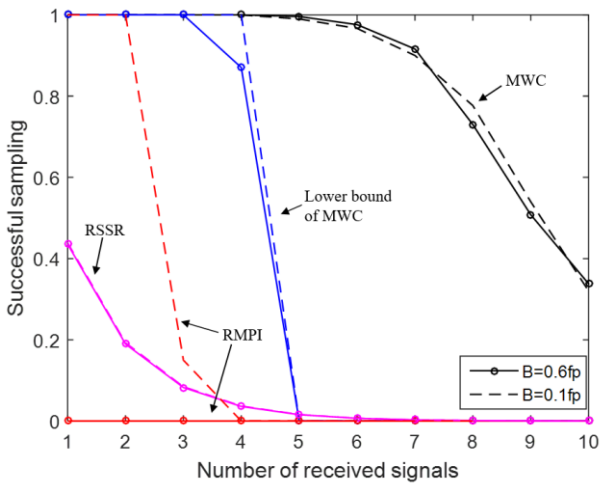

FIGURE 3. The probability of signal acquisition among the MWC, RMPI, and RSSR.

Fig. 3 shows that the MWC has the highest rate of signal acquisition. For a fair comparison, it was necessary to assign the same number of channels and sampling rates to all the receivers, including the RSSR. MWC and RMPI require a sampling rate of at least $f_s = qf_p$ for m channels. In other words, a necessary requirement for the total sampling rate is mqf_p. Because RSSR uses a single ADC with a sampling rate of W_{BPF}, we can set the ADC sampling rate to $W_{BPF} = mqf_p$. For the simulation, we set the conditions as $m = 4$, $f_{nyq} = 4Ghz, f_s = 220Mhz, f_p = 31.5Mhz, T_{acq} = 1.11\mu s$, and $B = 0.1f_p$ or $0.6f_p$. We acquired empirical simulation results from the MWC by the simultaneous orthogonal matching pursuit (SOMP) algorithm [15]. The simulation found that the probability that many samples will be split signals was lower than it would have been in theory because superposition is avoided when the test signal is generated. As shown in Fig. 3, compared to the MWC's performance at $\kappa_{MWC} = 4$, the RMPI could not acquire the signals with $B = 0.6f_p$ even though the more successful sampling criteria with $\kappa_{RMPI} = 9$ was applied. For that signal bandwidth, high sparsity occurred, which cannot be recovered by the SOMP algorithm. This advantage of the MWC is one reason that we adopted it for our radar ES system design. In addition, use of (13) helped facilitate the design process by allowing easy prediction of the system's signal-acquisition performance in terms of system parameters.

IV. SPLIT-SYNTHESIS METHOD

The high computational complexity makes the signal reconstruction consumes longer time and may result in failure in continuous signal acquisition. A failure occurs when the signal reconstruction time for the acquired sample obtained over the preceding acquisition time exceeds the acquisition time for the next sample acquisition. Even for the SOMP algorithm [15] which is one of the simplest signal reconstruction algorithms, the reconstruction time can easily exceed the acquisition time. Thus, to reduce the rate of failure of continuous signal reconstruction over a long acquisition time, careful new design on reducing the computational complexity is needed. Here we propose a split and synthesis method. Given a long signal acquisition time, the split-synthesis method trades-offs the computational complexity with the performance of signal reconstruction. Fig. 4 depicts the split-synthesis method.

A. SPLIT-PROCESS

After the MWC samples an aggregated radar signal over a long acquisition time T_{acq}, for example $0.13msec$ [9], the radar ES system imposes a uniform grid on the acquisition time at intervals of time slot T_{slot}. The aggregated radar signals in (1) are then reformulated as follows:

$$x(t) = \sum_{j=1}^{G} x_j(t - (j-1)T_{slot}) \qquad (18)$$

for $0 \le t < T_{slot}$, where $x_j(t)$ corresponds to the slice of aggregated radar signal in the j-th time slot. The number of time slots G is chosen to reduce computational complexity, and this choice is discussed later in this section. For the j-th time slot, the MWC output (3) can be expressed as follows:

$$\mathbf{Y}_j[n'] = \mathbf{C}\mathbf{Z}_j[n'], \qquad (19)$$

where the measurement matrix is $\mathbf{Y}_j \in \mathbb{R}^{m\times\tilde{l}_d}$, $\mathbf{C} \in \mathbb{C}^{m\times L}$ is the sensing matrix, $\mathbf{Z}_j \in \mathbb{R}^{L\times\tilde{l}_d}$ contains information of the aggregated radar signal, and

$$\tilde{l}_d = \frac{T_{slot}}{T_s} = q \cdot \frac{T_{slot}}{T_p} = q \cdot l_d. \qquad (20)$$

The relation (19) can be represented in matrix form as follows:

$$\begin{pmatrix} y_{j,1}[1] & \cdots & y_{j,1}\left[\tilde{l}_d\right] \\ \vdots & & \vdots \\ y_{j,m}[1] & \cdots & y_{j,m}\left[\tilde{l}_d\right] \end{pmatrix} = \begin{bmatrix} c_{1,-L_0} & \cdots & c_{1,0} & \cdots & c_{1,L_0} \\ \vdots & & \vdots & & \vdots \\ c_{m,-L_0} & \cdots & c_{m,0} & \cdots & c_{m,L_0} \end{bmatrix}$$

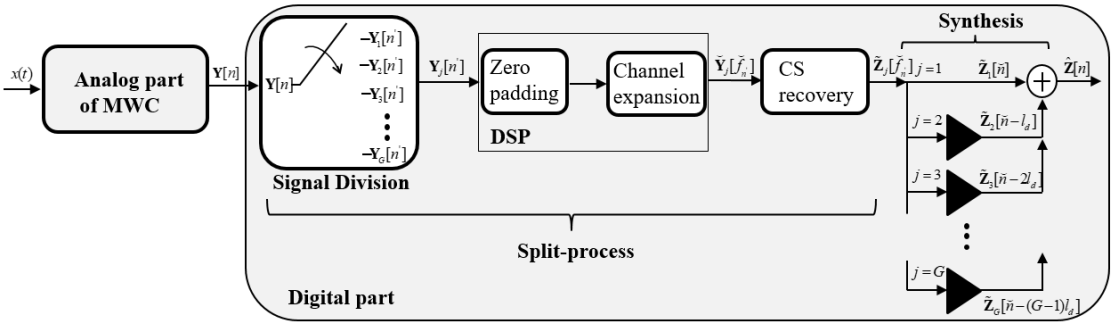

FIGURE 4. Block diagram of the proposed radar electronic surveillance system.

$$\times \begin{bmatrix} z_{j,-L_0}[1] & \cdots & z_{j,-L_0}[\tilde{l}_d] \\ \vdots & & \vdots \\ z_{j,0}[1] & \cdots & z_{j,0}[\tilde{l}_d] \\ \vdots & & \vdots \\ z_{j,L_0}[1] & \cdots & z_{j,L_0}[\tilde{l}_d] \end{bmatrix} \tag{21}$$

The next step is to extend the number m of channels in (19).

We present a straightforward channel expansion method to enlarge the rows of the measurement matrix $\mathbf{Y}_j$ and the sensing matrix $\mathbf{C}$ in (19); we then adopt the zero-padding technique that alleviates time aliasing discussed Section II-D. Before expanding the channels, qk zeros are added to the right side of each row of $\mathbf{Y}_j$ in (21), where $k < l_d$. Thereafter, as presented at (3), we exploit the way in which the $q = f_s/f_p$ sub-bands are piled in a single row of the $\mathbf{Z}_j$ matrix. By disassembling the q piled sub-bands, the rows of $\mathbf{Y}_j$ and $\mathbf{C}$ can be expanded via a fast Fourier transform (FFT) and simple matrix reorganization. If the zero-paddings before the FFT are not included, severe time aliasing occurs because the results from FFT beyond $\tilde{l}_d$ are lost, whereas they should be retained for the next timeslot. Thus, we can begin with padding zeros and performing the FFT on the right side of (21) to change the column indices of $\mathbf{Y}_j$ as the frequency axis. In other words, $y_{j,i}[n']$ becomes $y_{j,i}[f_{n'}]$ for $f_{n'} = 1, 2, \ldots, \tilde{l}_d + qk$.

By disjointing q piled sub-bands for the i-th row, we reorganize $\mathbf{Y}_j$ to be a $qm \times (l_d + k)$ matrix such that

$$\breve{y}_{j,i+v}[\breve{f}_{n'}] = \sum\nolimits_{v=0}^{q-1} y_{j,i}\left[v \cdot (l_d + k) + f_{n'}\right] \tag{22}$$

for $\breve{f}_{n'} = 1, 2, \ldots, l_d + k$. In the sensing matrix $\mathbf{C}$, by disjointing $q-1$ repeated $c_{i,l}$ times, such that $c_{i,M_0+s} = c_{i,-M_0+(s-1)}$ for $s \in [-q_0 + 1, q_0]$, $\mathbf{C}$ is also expanded as follows:

$$\breve{c}_{i+v,l} = \sum\nolimits_{v=0}^{q-1} c_{i,-L_0+v+l} \tag{23}$$

for $l = 0, 1, \ldots, M$. Consequently, with the channel expansion step, the relationship at (19) is transformed as follows:

$$\breve{\mathbf{Y}}_j[\breve{f}_{n'}] = \breve{\mathbf{C}}\breve{\mathbf{Z}}_j[\breve{f}_{n'}], \tag{24}$$

where $\breve{\mathbf{Y}}_j \in \mathbb{R}^{mq\times(l_d+k)}$, $\breve{\mathbf{C}} \in \mathbb{C}^{mq\times M}$, and $\breve{\mathbf{Z}}_j \in \mathbb{R}^{M\times(l_d+k)}$. The equal effect of qm enlarged equations helps to recover the input signals [14].

Compared to the conventional convolution method of (4), computational complexity is reduced by FFT expansion. For one channel, the computational complexity of the convolution method is $O\left(\tilde{l}_d^2\right)$, whereas the FFT method reduces it to $O\left(\tilde{l}_d \log \tilde{l}_d\right)$. When the FFT is performed in tandem with the split process, the computational complexity is reduced to $O\left(\left(\tilde{l}_d + Gk\right) \log\left(\tilde{l}_d/G + k\right)\right)$. Because the ES system samples radar signals over a long acquisition time, the effect of k additional zeros is negligible, i.e., $k \ll \tilde{l}_d$. To reduce the computational complexity, the number of timeslots G can be calculated as follows:

$$G = \arg\min_{G\in\mathbb{N}} \left(\tilde{l}_d + Gk\right) \log\left(\tilde{l}_d/G + k\right). \tag{25}$$

For example, when $l_d = 256$, $k = 2$, and $G = 76$, the computational complexities of the convolution expansion, FFT alone, and FFT with signal division are 65536, 2048, and 685, respectively. The reduced computational complexity of the split process shortens the system's computation time.

B. SYNTHESIS PROCESS

A CS algorithm recovers the signal information as $\tilde{\mathbf{Z}}_j[\breve{f}_{n'}] \in \mathbb{R}^{4N\cdot(l_d+k)}$ by solving the MMV problem of (24), while $\tilde{\mathbf{Z}}_j[\breve{n}]$ is generated by applying an inverse of FFT. The procedures from the split process through generation of $\tilde{\mathbf{Z}}_j[\breve{n}]$ are repeated for each of the G timeslots, and the results from all the timeslots are synthesized as follows:

$$\hat{\mathbf{Z}}[n] = \sum\nolimits_{j=1}^{G-1} \tilde{\mathbf{Z}}_j[\breve{n} - (j-1)l_d] + \tilde{\mathbf{Z}}_G[\breve{n} - (G-1)l_d], \tag{26}$$

where the matrix $\tilde{\mathbf{Z}}_G$ of the last timeslot decimates the columns in $[l_d + 1, l_d + k]$. As depicted in Fig. 4, each $\tilde{\mathbf{Z}}_j$ is delayed for l_d using buffers and then synthesized such that the $[l_d + 1, l_d + k]$ columns of $\tilde{\mathbf{Z}}_{j-1}$ are added to the k front- columns of $\tilde{\mathbf{Z}}_j$ to alleviate the time-aliasing. With (22), (23) and the synthesis process, we address the time-aliasing, as verified in Section VI.

Time-wise information, including PRI, TOA, and TOD, can be found from the reconstructed radar waveform or the estimation method presented in [16]. The carrier frequencies can be estimated with pulse spectrum density estimation [17].

Direction-of-arrival (DOA) can also be estimated using a crossed-loop/monopole antenna and a multiple signal classification (MUSIC) algorithm [18].

TABLE 1. Parameters of the radar ES system.

Parameters (Symbol)	Relationship	Value
Acquisition time (T_{acq})	$T_{acq} = G \cdot T_{slot}$	0.1302 *ms*
The number of time slots (G)	-	100
Nyquist frequency (f_{nyq})	$f_{nyq} \geq f_{\max}$	4 *GHz*
Bandwidth (B)	$B_{\min} \leq B \leq B_{\max}$	$\leq$ 31.49 *MHz*
◊ Channel expansion factor (q)	> 0	7
◊ Period of PR sequences (T_p)	$T_p = 1/f_p$	0.03176 *ns*
◊ ADC sampling rate (f_s)	$f_s = q \cdot f_p$	220 *MHz*
◊ Number of PR pattern (M)	$M = L - q + 1$	127
◊ Physical channels (m)	-	4
◊ Virtual channels ($\breve{m}$)	$\breve{m} = mq$	28

The dependent parameters are denoted as ◊ for a given hardware.

The parameters of the proposed system are listed in Table 1. For a given analog system, the PR sequence parameters, ADC sampling rate, and number of channels are the dependent parameters. The long acquisition time T_{acq} used to capture reliable radar signals rapidly increases the computational complexity in the digital signal reconstruction. Note that the long acquisition time also improves frequency resolution. However, the split-synthesis process can reduce the reconstructing time. In addition to the split-synthesis process over the long acquisition time, we provide a sub-sampling method to reduce the computational complexity of MMV algorithm for every timeslot.

V. MMV ALGORITHM PRE-PROCESSING

This section proposes a sub-sampling method which uses pre-processing to proportionally reduce the computational complexity of the MMV recovery algorithm in each timeslot. As discussed in the previous section, the radar ES system could greatly reduce the computational complexity of the channel expansion by splitting a long period of acquisition time into discrete timeslots. However, because there are still unnecessary measurement vectors in (24) and the total computational complexity of MMV recovery for G timeslots is still high owing to the long acquisition time, the reconstruction time can still exceed the acquisition time and cause bottlenecks. Because the MMV recovery algorithm involves matrix multiplication and/or inversion, the computational complexity of the algorithm rapidly increases with the number of measurement vectors. In addition, [19] shows that the recovery performance of the MMV algorithm is saturated with the number of measurements. Thus, we propose a sub-sampling method as a preliminary step to reduce the computational complexity of the following MMV algorithm. This method strategically selects a subset of measurement vectors without missing the support set which indicate the indices of nonzero sub-bands. The sub-sampling method is detailed in Section V-A and the benefits in terms of computational complexity and support recovery performance are presented in Section V-B.

A. SUB-SAMPLING METHOD

By the linearity of (24), selecting columns of $\breve{\mathbf{Y}}_j$ is equivalent to selecting columns of the signal matrix $\breve{\mathbf{Z}}_j$. We therefore select the columns of $\breve{\mathbf{Y}}_j$ based on the structure of the signal matrix $\breve{\mathbf{Z}}_j$. The rows of $\breve{\mathbf{Z}}_j$ contain spectrally orthogonal sub-bands of the discrete spectrum of $x(t)$ at intervals of f_p. From the discrete Fourier transform, the column indices represent the frequency grid in intervals of $1/T_{slot}$. Each narrow-band spectrum of $x_j(t)$ is contained within the rows. Some of the narrow-band spectra may be split by the borderline of the sub-bands based on their center frequencies.

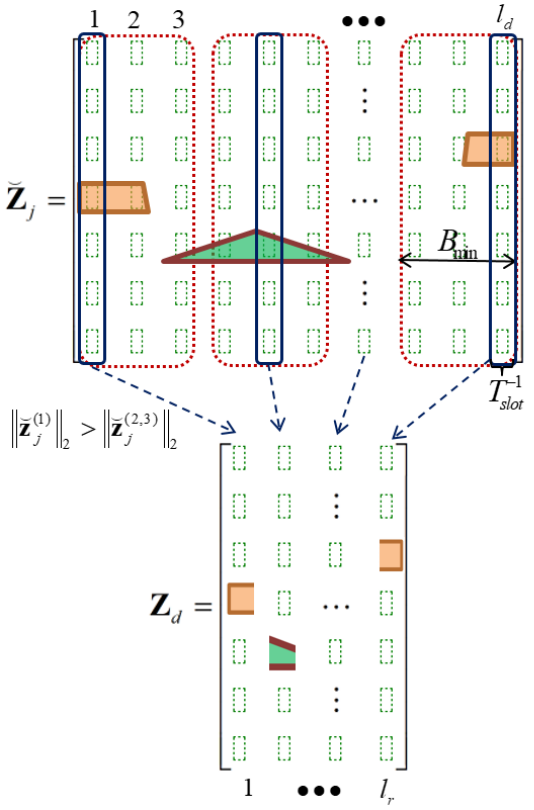

FIGURE 5. Selected columns of measurement matrix contain essential signal information for detecting a support set while reducing computational burden.

To address this scenario, we propose the sub-sampling method depicted in Fig. 5. This method generates subsets by classifying columns of $\breve{\mathbf{Y}}_j$ at intervals less than the minimum signal bandwidth, $B_{\min}$. For each subset, the sub-sampling method selects the column that has the maximum energy. When the subset comprises fewer columns than $B_{\min}$, the method avoids the situation where several signals are present in a subset and do not overlap in columns. In this situation, only one of the signals within the sampling window

will be selected, whereas the others are missed. However, a sub-sampled matrix $\mathbf{Y}_d \in \mathbb{R}^{mq \times l_r}$, the union of selected columns, includes components of all of the signals while still reducing the size of the measurement matrix. The number of sub-sampled columns is calculated as follows:

$$l_r = \lceil l_d / \lfloor B_{\min} T_{sub} \rfloor \rceil, \tag{27}$$

where $\lfloor B_{\min} T_{sub} \rfloor$ is the element number of each subset. The notation $\check{\mathbf{Z}}_j$ also becomes $\mathbf{Z}_d \in \mathbb{R}^{M \times l_r}$. Because this simple sub-sampling method works in one step before the following iterative MMV recovery algorithm, the computational complexity added by the sub-sampling is negligible. The reduced column l_r reduces computational complexity proportionally in the following MMV recovery algorithm. We chose the SOMP algorithm [15] as an example to verify the computational complexity benefits and the recovery performance of the support set.

B. DISCUSSION ON COMPUTATIONAL COMPLEXITY

To verify the computational complexity benefit of our sub-sampling method, we adopted the SOMP algorithm [15], which is commonly used to solve MMV problems. Note that the sub-sampling method is independent of SOMP. Although there are advanced MMV algorithms, such as MMV basic matching pursuit (M-BMP), Regularized MMV FOCUS (M-FOCUS), Bayesian, and group OMP (GOMP), these are inappropriate for our radar ES system because M-BMP has problems with signal reconstruction performance, and the other algorithms require high computational complexity. To implement our radar ES system with field programmable gate array, the high computational complexity becomes a problem. M-BMP works by matching a column of the sensing matrix with measurement vectors. However, according to terminal conditions, the algorithm provides an accurate solution with high sparsity or an inaccurate solution when the algorithm terminates with a predetermined sparsity amount [20]. Meanwhile, the other algorithms require higher computational complexities compared to SOMP [20]–[22]. Regularized M-FOCUS algorithms contain a concatenation of three matrices compared to the two matrices required of SOMP. Bayesian has a conversion of MMV to single measurement vector, and the dimension of the sensing matrix is increased with the number of measurements [22]. The number of rows and columns of the sensing matrix in GOMP are proportionally increased with the group size parameter [21]. From these reasons, we adopted SOMP because it not only shows the effect of our sub-sampling method but also it requires low complexity.

The SOMP is an iterative algorithm. At each iteration, the algorithm recovers the indices of nonzero rows of a signal matrix $\mathbf{Z}_d$, i.e., the support set, in (24) by matching the MMV matrix $\mathbf{Y}_d$ with the bases of the sensing matrix $\check{\mathbf{C}}$. The procedure of SOMP is adjusted for the radar ES system to enhance the algorithm's efficiency and reduce computational complexity. The terminal condition is

$$\|\mathbf{Y}_d\|_2 \leq EPS. \tag{28}$$

When (28) is satisfied, SOMP determines that signals do not exist. Until this condition is satisfied, the algorithm continues to estimate a support among a set Λ, defined as row indices of $\mathbf{Z}_d$, which is expressed as follows:

$$J = \arg\max_{\Lambda} \left\| \mathbf{C}_{\Lambda}^{H} \mathbf{Y}_{residue}[i] \right\|_2, \tag{29}$$

where $\mathbf{C}_{\Lambda}$ is a column of $\check{\mathbf{C}}$ and i is the iteration index. In the first iteration, the original MMV $\mathbf{Y}_d$ replaces the residual matrix $\mathbf{Y}_{residue}$. From the conjugate symmetry of a real-valued radar signal, the selected and symmetric supports can be stored in S_i gathered at S, i.e., $S = \{S_i | \, i = 1, 2, \ldots, N\}$. After estimating the support set S containing $2i$ elements, the residual of $\mathbf{Y}_d$ is generated by the following equation:

$$\mathbf{Y}_{residue} = \mathbf{Y}_d - \mathbf{C}_S \cdot \mathbf{C}_S^{\dagger} \mathbf{Y}_d, \tag{30}$$

where $\mathbf{C}_S^{\dagger}$ is a Moore–Penrose pseudoinverse of the outcome by extracting the columns of S from $\check{\mathbf{C}}$ in (24). Note that N real-valued radar signals can yield up to $4N$ supports. SOMP detects the support set Ω for the upmost $2N$ iterations instead of $4N$ iterations. The signal information is reconstructed as follows:

$$\tilde{\mathbf{Z}}_j[\check{f}_n] = \mathbf{C}_{\Omega}^{\dagger} \cdot \check{\mathbf{Y}}_j[\check{f}_n]. \tag{31}$$

The result of (31) can be used for the synthesis process explained in Section IV-C.

To verify computational complexities, we focus on the matrix multiplication and inverse operations (29) and (30) in the algorithm because these are the main factors that enlarge computational complexity. For a time slot, the sizes of the measurement and sensing matrices are $\check{m} \times l_d$ and $\check{m} \times M$, respectively, where $\check{m} = mq$. For (29), the computational complexity is $O(M\check{m}l_d)$. In (30), the computational complexities are different for each i-th iteration owing to $\mathbf{C}_S \in \mathbb{C}^{\check{m} \times 2i}$, but we can ignore this effect for easy verification as long as $i < \check{m}$. Thus, the computational complexity of (30) becomes $O(\check{m}^2(l_d + 2) + 16\check{m})$. As a result, the total complexity for N signals becomes

$$O\left(2N\left(l_d \check{m}\left(M + \check{m} + 2\right) + 16\check{m}\right)\right). \tag{32}$$

Next, we compute the computational complexity of the preprocessing method. The computational complexity becomes

$$O\left(2N\left(l_r \check{m}\left(M + \check{m} + 2\right) + 16\check{m}\right)\right), \tag{33}$$

where $l_r < l_d$ is the number of sub-sampled columns. In (33), we see the computational complexity reduced in proportion to the small l_r.

Fig. 6 plots the support recovery rate versus the number of sub-sampled columns of the measurement matrix. The support recovery rate is defined as one when the recovered support set is a subset of the original signal. We simulated

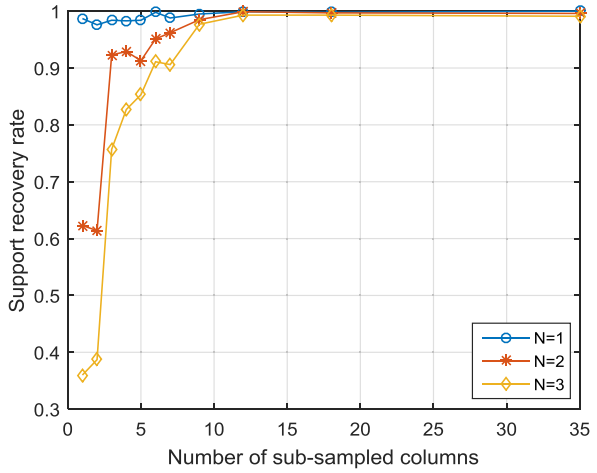

FIGURE 6. Support recovery rate versus the number of sub-sampled columns of measurement matrix using SOMP.

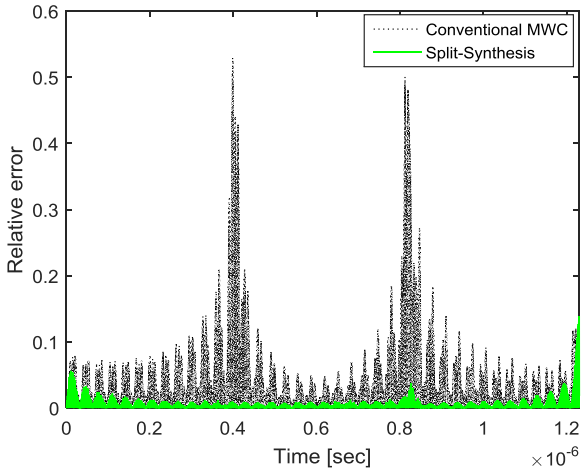

FIGURE 7. The relative errors at the borders of the timeslots are alleviated with the split-synthesis process of the proposed radar ES system.

the support recovery rate along the number of subsets corresponding to the number of sub-sampled columns compared to the original columns, $l_d = 35$. The minimum bandwidth of the signal was $B_{\min} = 0.1 f_p = 3.15 MHz$. From (27), l_r is *12*, which is a similar recovery performance to original full columns as shown in Fig. 6. This implies that the sub-sampled MMV $\mathbf{Y}_d$ does not miss the signal information and includes all of the essential parts of the original MMV $\breve{\mathbf{Y}}_j$. In this scenario, the sub-sampling method reduced computational complexity by a third. Consequently, we can conclude that this sub-sampling method proportionally reduces computational complexity while maintaining recovery performance.

VI. SIMULATIONS

Through simulations, we verified that the radar ES system can successfully trade-off between the reduction of computational complexity and degradation of signal reconstruction performance. For the simulations, we generated three pulsed radar signals whose carrier frequencies appeared randomly from $f_{\min} = 0.5 GHz$ to $f_{\max} = 2 GHz$. We gave as an input 5 dB pulsed radar signals where the signal to noise ratio (SNR) and signal type were not discussed. The SNR is defined as $10 \cdot \log\left(\|x\|_2^2 / \|n\|_2^2\right)$, where x and n are the input signals and noise vectors, respectively. We considered a four-channel MWC system; the remaining system parameters are listed in Table 1. The SOMP algorithm discussed in Section V was used to reconstruct the multiband signal.

First, we tested the improvement to the relative error in the reconstructed signal gained by the split-synthesis process of the radar ES system. In this simulation, the relative error was defined as follows:

$$relative\_error[i] := \|x[i] - x_r[i]\|_2^2, \tag{34}$$

where $x[i]$ is the input radar value at the i-th time and x_r is the reconstructed radar vector. To clearly verify the reduction of the relative errors at the borders of the timeslots, we shortened

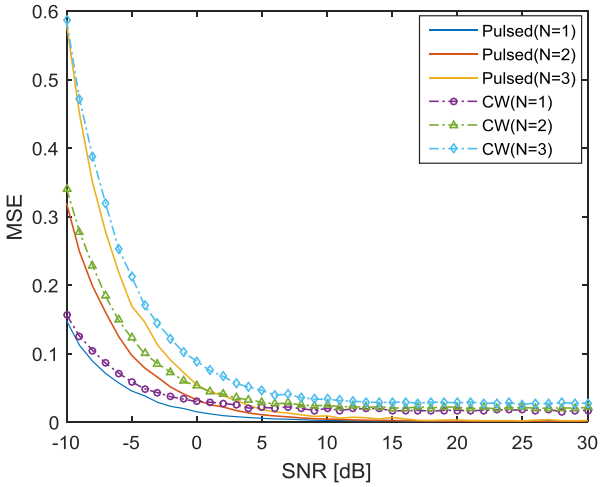

FIGURE 8. Reconstruction performance of radar ES system with pulsed signal and continuous wave (CW) for varying SNRs.

the acquisition period $GT_{slot} = 1.29 \mu s$. As shown in Fig. 7, the errors among the timeslots are clearly reduced with the split-synthesis process. Although the trade-off parameter k discussed at the Section IV-A yields k additional columns in the channel-expanded measurement matrix, compared to the original column number $l_d = 35$, our simulation showed that even a small $k = 2$ yields some benefit. The Table 2 compares computational complexity between the conventional MWC and the split-synthesis process of the proposed radar ES system. Note that the order of computational complexity was discussed at the Section IV-A. With the small trade-off parameter $k = 2$, the split-synthesis of (22)-(26) can considerably reduce the computational complexity at the cost of negligible degradation of signal reconstruction as shown in the Fig. 7.

Second, we verified the robustness of noise along SNRs for continuous waves (CWs) and pulsed signals [9]. In this simulation, the MSE is defined as $\|x - x_r\|_2^2 / \|x\|_2^2$. As can be seen in Fig. 8, the pulsed signal was reconstructed better than

TABLE 2. Comparison of computational complexity.

	Conventional MWC	Split-Synthesis
Order of complexity	$O\left(G^2 l_a^{\,2}\right)$	$O\left(\left(\tilde{l}_a + Gk\right)\log\left(\tilde{l}_a / G + k\right)\right)$
Calculated complexity	11,025	155

The simulation parameters are $l_a = 35$, $G = 3$ and $k = 2$, which are also used in Fig. 7.

the CW. For the purpose of this study, our radar ES system can successfully monitor up to three radar signals above 2 dB as we pursued the detection of three radar signals under 5% of the MSE.

VII. CONCLUSION

In this study, we verified and compared the signal-acquisition performances among RSSR, RMPI, and MWC with a novel probability analysis. In the analysis, the MWC performed better than the other receivers. In addition, this analysis may be extended for comparison between CS-based sub-Nyquist receivers. Our proposed radar ES system with MWC was able to monitor incoming wideband signals in a simulation. In this ES system, the split-synthesis process considerably reduced the computational complexity with the trade-off parameter to alleviate the degradation of signal reconstruction. Pre-processing with sub-sampling before the MMV algorithm was able to proportionally reduce computational complexity while maintaining signal recovery performance. We plan to implement and test this signal-acquisition methods using the hardware that is currently being developed. As a future work, it would be meaningful to consider the problem of estimating the PDW of radar signals, including spatial location of carrier frequencies.

REFERENCES

[1] G. Schrick and R. G. Wiley, "Interception of LPI radar signals," in *Proc. Radar Conf.*, May 1990, pp. 108–111.
[2] A. B. Carlson, P. B. Crilly, and J. C. Rutledge, *Communication Systems: An Introduction to Signals and Noise in Electrical Communication*, 4th ed. New York, NY, USA: McGraw-Hill, 2002.
[3] M. Mishali and Y. C. Eldar, "From theory to practice: Sub-Nyquist sampling of sparse wideband analog signals," *IEEE J. Sel. Topics Signal Process.*, vol. 4, no. 2, pp. 375–391, Apr. 2010.
[4] M. Mishali, Y. C. Eldar, O. Dounaevsky, and E. Shoshan, "Xampling: Analog to digital at sub-Nyquist rates," *IET Circuits, Devices and Syst.*, vol. 5, no. 1, pp. 8–20, 2011.
[5] J. Yoo, S. Becker, M. Monge, M. Loh, E. Candes, and A. E. Neyestanak, "Design and implementation of a fully integrated compressed-sensing signal acquisition system," in *Proc. IEEE Int. Conf. Acoust., Speech Signal Process. (ICASSP)*, May 2012, pp. 5325–5328.
[6] J. Yoo *et al.*, "A compressed sensing parameter extraction platform for radar pulse signal acquisition," *IEEE Trans. Emerg. Sel. Topics Circuits Syst.*, vol. 2, no. 3, pp. 626–638, Sep. 2012.
[7] D. L. Donoho, "Compressed sensing," *IEEE Trans. Inf. Theory*, vol. 52, no. 4, pp. 1289–1306, Apr. 2006.
[8] E. J. Candès and T. Tao, "Decoding by linear programming," *IEEE Trans. Inf. Theory*, vol. 51, no. 12, pp. 4203–4215, Dec. 2005.
[9] M. A. Richards, J. Scheer, W. A. Holm, and W. L. Melvin, Eds., *Principles of Modern Radar*. Raleigh, NC, USA: SciTech, 2010.
[10] L. Bin, T. W. Rondeau, J. H. Reed, and C. W. Bostian, "Analog-to-digital converters," *IEEE Signal Process. Mag.*, vol. 22, no. 6, pp. 69–77, Nov. 2005.
[11] X. Liu, W. Li, J. Wei, and L. Cheng, "Adaptable hybrid filter bank analog-to-digital converters for simplifying wideband receivers," *IEEE Commun. Lett.*, vol. 21, no. 7, pp. 1525–1528, Jul. 2017.
[12] A. V. Oppenheim and R. W. Schafer, *Discrete-Time Signal Processing*, 3rd ed. Upper Saddle River, NJ, USA: Pearson, 2010.
[13] S. L. Miller and D. G. Childers, *Probability and Random Processes: With Applications to Signal Processing and Communications*, 1st ed. Burlington, NJ, USA: Elsevier, 2004.
[14] D. L. Donoho and M. Elad, "Optimally sparse representation in general (nonorthogonal) dictionaries via ℓ^1 minimization," *Proc. Nat. Acad. Sci. USA*, vol. 100, no. 5, pp. 2197–2202, 2003.
[15] J. A. Tropp, A. C. Gilbert, and M. J. Strauss, "Algorithms for simultaneous sparse approximation. Part I: Greedy pursuit," *Signal Process.*, vol. 86, no. 3, pp. 572–588, 2006.
[16] M. Mishali, Y. C. Eldar, and A. J. Elron, "Xampling: Signal acquisition and processing in union of subspaces," *IEEE Trans. Signal Process.*, vol. 59, no. 10, pp. 4719–4734, Oct. 2011.
[17] M. Mishali, A. Elron, and Y. C. Eldar, "Sub-Nyquist processing with the modulated wideband converter," in *Proc. IEEE Int. Conf. Acoust., Speech Signal Process. (ICASSP)*, Mar. 2010, pp. 3626–3629.
[18] Y. Tian, B. Wen, J. Tan, and Z. Li, "Study on pattern distortion and DOA estimation performance of crossed-loop/monopole antenna in HF radar," *IEEE Trans. Antennas Propag.*, vol. 65, no. 11, pp. 6095–6106, Nov. 2017.
[19] Y. C. Eldar and H. Rauhut, "Average case analysis of multichannel sparse recovery using convex relaxation," *IEEE Trans. Inf. Theory*, vol. 56, no. 1, pp. 505–519, Jan. 2010.
[20] S. F. Cotter, B. D. Rao, K. Engan, and K. Kreutz-Delgado, "Sparse solutions to linear inverse problems with multiple measurement vectors," *IEEE Trans. Signal Process.*, vol. 53, no. 7, pp. 2477–2488, Jul. 2005.
[21] A. T. Abebe and C. G. Kang, "Iterative order recursive least square estimation for exploiting frame-wise sparsity in compressive sensing-based MTC," *IEEE Commun. Lett.*, vol. 20, no. 5, pp. 1018–1021, May 2016.
[22] Z. Zhang and B. D. Rao, "Sparse signal recovery with temporally correlated source vectors using sparse Bayesian learning," *IEEE J. Sel. Topics Signal Process.*, vol. 5, no. 5, pp. 912–926, Sep. 2011.

JEONG PARK received the undergraduate degree in electrical engineering and computer science from the Kyungpook National University, Daegu, South Korea, in 2015. He is currently pursuing the M.S. degree with the School of Electrical Engineering and Computer Science, Gwangju Institute of Science and Technology, South Korea. His research interests include sub-Nyquist sampling, compressed sensing, estimation, and wireless communication.

JEHYUK JANG received the B.S degree in electronic engineering from the Kumoh National Institute of Technology, Gumi, South Korea, in 2014, and the M.S degree in information and communication engineering from the Gwangju Institute of Science and Technology, where he is currently pursuing the Ph.D. degree with the School of Electrical Engineering and Computer Science. His research interests include sub-Nyquist sampling and compressed sensing.

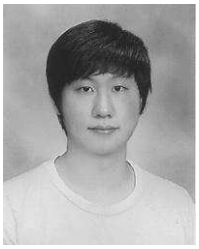

SANGHUN IM received the B.S. degree in electronics engineering from Soongsil University, Seoul, South Korea, in 2009, and the M.S. and Ph.D. degrees in electrical engineering from the Korea Advanced Institute of Science and Technology, Daejeon, South Korea, in 2011 and 2016, respectively. He is currently with Hanwha Systems, South Korea. His current research interests include communication theories and signal processing for wireless communications, and physical layer security.

HEUNG-NO LEE (SM'13) received the B.S., M.S., and Ph.D. degrees from the University of California, Los Angeles, CA, USA, in 1993, 1994, and 1999, respectively, all in electrical engineering. He was with the HRL Laboratories, LLC, Malibu, CA, USA, as a Research Staff Member from 1999 to 2002. From 2002 to 2008, he was an Assistant Professor with the University of Pittsburgh, PA, USA. In 2009, he then moved to the School of Electrical Engineering and Computer Science, Gwangju Institute of Science and Technology, South Korea, where he is currently affiliated. His areas of research include information theory, signal processing theory, communications/networking theory, and their application to wireless communications and networking, compressive sensing, future internet, and brain–computer interface. He has received several prestigious national awards, including the Top 100 National Research and Development Award in 2012, the Top 50 Achievements of Fundamental Researches Award in 2013, and the Science/Engineer of the Month in 2014.